ON THE STRUCTURE AND STABILIZATION MECHANISMS OF PLANAR AND CYLINDRICAL PREMIXED FLAMES

James A. Eng, Delin Zhu, and Chung K. Law
Department of Mechanical and Aerospace Engineering
Princeton University
Princeton, New Jersey 08544

Introduction

The configurational simplicity of the stationary one-dimensional flames renders them intrinsically attractive for fundamental flame structure studies. The possibility and fidelity of studies of such flames on earth, however, have been severely restricted by the unidirectional nature of the gravity vector. To demonstrate these complications, let us first consider the premixed flame. Here a stationary, one-dimensional flame can be established by using the flat-flame burner (Fig. 1a). This flame, however, is inherently nonadiabatic because it is stabilized through heat loss to the burner surface. Furthermore, radicals generated at the flame potentially can also diffuse back to the burner surface and become deactivated. Such loss processes have introduced uncertainties in the study of flame chemistry. Furthermore, even an adiabatic planar flame can be produced by using the counterflow burner (Fig. 1b), where two symmetrical planar flames are formed in the stagnation field of two opposed jets of premixed gases, the flame is aerodynamically strained by the nonuniform flow field. The associated flame stretch effects can significantly modify the flame properties from the idealized one-dimensional flame in the doubly-infinite domain [1].

A class of one-dimensional flames that has the potential of eliminating heat loss and stretch effects is the cylindrical and spherical flames, where a premixed gas flows through a porous cylindrical (or spherical) burner and the resulting flame is formed at some distance from the burner, as shown in Figs. 1c and 1d. Since the flame is stationary and the flow velocity is in the radial direction and thereby normal to the flame surface, it is curved but not stretched [1]. Furthermore, while the flame can be stabilized by heat loss to the burner, the divergent nature of the flow offers an additional stabilization mechanism. That is, as the flow rate is continuously increased the flame recedes from the burner and heat loss can be eventually reduced to become negligible as compared to the heat generated at the flame. At this point the flame temperature is almost equal to the adiabatic flame temperature. Further increases in the flow rate can be accommodated by an increase in the flame standoff distance to a position where the flame speed again balances the flow velocity. Thus, the cylindrical geometry offers a unique advantage for the study of adiabatic, one-dimensional, stretch-free flames that is not present in other commonly used experimental systems. It is, however, also clear that because of the distorting nature of the buoyant flow, such a flame can only be established, and studied, in a microgravity (μg) environment.

We next consider nonpremixed flames. First it may be noted that in an unbounded gravity-free environment, the only stationary one-dimensional flame is the spherical flame. Indeed, this is a major motivation for the study of microgravity droplet combustion, in which the gas-phase processes can be approximated to be quasi-steady because of the significant disparity between the gas and liquid densities for subcritical combustion. However, recent studies [2] have shown that because of initial conditions, the combustion response such as the droplet burning rate and the flame location still vary significantly with time. Such complications can be avoided by using the spherical porous burner of Fig. 1d, in which a truly steady spherical flame can be generated in μg by steadily feeding either a gaseous or a liquid fuel through the burner.

In view of the above considerations, an experimental and theoretical program on cylindrical and spherical premixed and nonpremixed flames in microgravity has been initiated. For premixed flames, we are interested in (1) assessing the heat loss versus flow divergence as the dominant stabilization mechanism, (2) determining the laminar flame speed by using this configuration, and (3) understanding the development of flamefront instability and the effects of flame curvature on the burning intensity. For nonpremixed flames, we are interested in the state of extinction and the properties of the soot layer formed in the inner region to the flame, as observed in microgravity droplet experiments [3]. For both premixed and nonpremixed flames the detailed dynamic, thermal, and chemical structures of the flame will also be studied through laser-based instrumentation and computation with detailed chemistry.

As a starting point for the present program, we have performed a computational and normal-gravity (ng) experimental investigation of the planar premixed flame over the flat flame burner, which serve as a calibrating and referencing system for the study of cylindrical flames. We have also performed theoretical, computational and μg experimental investigations of the cylindrical flame, and will present comparisons between the planar and cylindrical flames.

Asymptotic Analysis and Qualitative Behavior

The nondimensional conservation equations for the reactant mass fractions Y_i and temperature T can be expressed for the cylindrical flame as

$$\left[\tilde{m}\frac{d\tilde{Y}_F}{d\tilde{r}} - \frac{1}{Le_F}\frac{d}{d\tilde{r}}\left(\tilde{r}\frac{d\tilde{Y}_F}{d\tilde{r}}\right)\right] - \left[\tilde{m}\frac{d\tilde{Y}_O}{d\tilde{r}} - \frac{1}{Le_O}\frac{d}{d\tilde{r}}\left(\tilde{r}\frac{d\tilde{Y}_O}{d\tilde{r}}\right)\right] = 0 \tag{1}$$

$$\left[\tilde{m}\frac{d\tilde{Y}_F}{d\tilde{r}} - \frac{1}{Le_F}\frac{d}{d\tilde{r}}\left(\tilde{r}\frac{d\tilde{Y}_F}{d\tilde{r}}\right)\right] + \left[\tilde{m}\frac{d\tilde{T}}{d\tilde{r}} - \frac{d}{d\tilde{r}}\left(\tilde{r}\frac{d\tilde{T}}{d\tilde{r}}\right)\right] = 0 \tag{2}$$

$$\tilde{m}\frac{d\tilde{Y}_F}{d\tilde{r}} - \frac{1}{Le_F}\frac{d}{d\tilde{r}}\left(\tilde{r}\frac{d\tilde{Y}_F}{d\tilde{r}}\right) = -\frac{\Lambda}{\varepsilon^2(\tilde{\beta}_O - 1)}\tilde{r}\tilde{\rho}^2\tilde{Y}_F\tilde{Y}_O\exp\left[\frac{\tilde{T}_f}{\varepsilon}\left(\frac{\tilde{T} - \tilde{T}_f}{\tilde{T}}\right)\right] \tag{3}$$

In the above the nondimensional quantities are $\tilde{r} = r/r_S$, $\tilde{m} = mc_P/2\pi\lambda$, $\tilde{Y}_F = Y_F/\beta_F$, $\tilde{Y}_O = Y_O/\mu_O\beta_O$, $Le_i = \lambda/c_P\rho_S D_i$ is the Lewis number of the ith specie, $\tilde{T} = c_P T/q_F$, $\tilde{\rho} = \rho/\rho_f$, $\tilde{\beta}_O = \beta_O/m_O\beta_F$, Λ is the burning rate eigenvalue, and $\varepsilon = \tilde{T}_f/\tilde{T}_a$ is the small expansion parameter, where T_a is the activation temperature. Furthermore, r is the radial coordinate, r_S the burner radius, β_i the mass flux fraction of the ith specie at the burner surface, μ_O is the stoichiometric mass ratio between oxygen and fuel, ρ the density, c_P the mixture specific heat, λ the thermal conductivity, D_i the mass diffusivity of the ith specie, q_F the energy release per unit mass of fuel consumed, and m the mass flow rate per unit burner length. The boundary conditions are

$$\tilde{r} = 1 \;:\; \tilde{T} = \tilde{T}_s \qquad \tilde{m}\tilde{Y}_F - \frac{1}{Le_F}\tilde{r}\frac{d\tilde{Y}_F}{d\tilde{r}} = \tilde{m} \qquad \tilde{m}\tilde{Y}_O - \frac{1}{Le_O}\tilde{r}\frac{d\tilde{Y}_O}{d\tilde{r}} = \tilde{m}\tilde{\beta}_O \tag{4}$$

$$\tilde{r} \to \infty : \quad \tilde{T},\ \tilde{Y}_i \text{ bounded} \tag{5}$$

where T_S is the burner surface temperature. The analysis was restricted to a fuel lean system with a one-step irreversible reaction. The problem is now well defined, and the analysis proceeds using the standard techniques of asymptotic analysis [4], with ε as the small expansion parameter.

The proper independent variable for the system is the mass flow rate m, with the overall flame response being the flame temperature, the standoff distance from the burner, and the heat loss to the burner. The analysis yields the following expressions relating the nondimensional flame temperature $\tilde{T}_f$, flame radius $\tilde{r}_f$, and burner heat loss $\tilde{L}$ to the normalized mass flow rate $M = \tilde{m}/\tilde{m}^o$ for the cylindrical geometry,

$$M = \frac{\tilde{m}}{\tilde{m}^o} = \tilde{r}_f \frac{\tilde{T}_f}{\tilde{T}_{ad}} \exp\left[\frac{1}{2}\tilde{T}_a\left(\frac{1}{\tilde{T}_{ad}} - \frac{1}{\tilde{T}_f}\right)\right] \tag{6}$$

$$\frac{\tilde{T}_f}{\tilde{T}_{ad}} = 1 - \frac{1}{\tilde{T}_{ad}}\left(\frac{1}{\tilde{r}_f^{\tilde{m}}}\right) \tag{7}$$

$$\tilde{L} = \frac{\tilde{m}}{\tilde{m}^o}\left(\tilde{T}_{ad} - \tilde{T}_f\right) = \frac{\tilde{m}}{\tilde{m}^o}\left(\frac{1}{\tilde{r}_f^{\tilde{m}}}\right) \tag{8}$$

where T_{ad} is the adiabatic flame temperature and $m^o = 2\pi r_s \rho_s S_u^o$ is a reference flow rate based on the laminar flame speed. Note that due to divergence M can have a value greater then one. The nondimensional heat loss is $\tilde{L} = L/m^o \beta_F q_F$, where L is the heat transfer to the burner, and can be interpreted as the energy transferred to the burner per unit reference energy of the mixture.

Figures 2 to 4 are graphs of the heat loss $\tilde{L}$, flame standoff distance $\Delta = r_f - r_s$, normalized flame temperature $\bar{T}_f = \tilde{T}_f / \tilde{T}_{ad}$ and heat loss per unit mass as a functions of M. In order to present the results for the planar and cylindrical geometries on the same graph, the standoff distances are normalized by the laminar flame thickness $\delta^o = \lambda/c_p \rho_s S_u^o$, rather than by the burner radius. Figures 2 and 3 show that the standoff position and the total heat loss rate display a dual response behavior in that the heat loss has a maximum and the flame standoff position has a minimum. This behavior has been observed experimentally [5,6] and explained theoretically [7] for the planar flame.

For the planar case M is bounded by one, at which the flame moves to infinity, the heat loss to the burner vanishes, and the flame speed is S_u^o. On the other hand, for the cylindrical flame M can be increased beyond one due to flow divergence. Consequently, the flame is located at a finite standoff position even after the heat loss has become vanishingly small. The stabilization mechanism has therefore changed from heat loss to flow divergence. Comparing the results of the two cylindrical flames with different burner radii, the flame with the smaller burner is stabilized closer to the burner because of the larger divergence effect of the smaller burner.

It is also of interest to examine the mass flux through the reaction zone and compare it with the reference laminar flame value. An expression for this can be obtained by normalizing the mass flow by a reference mass flow rate based on the reaction zone area, $m_f^o = 2\pi r_f \rho_s S_u^o$. The resulting expression is

$$\frac{\tilde{m}}{\tilde{m}_f^o} = \frac{\tilde{T}_f}{\tilde{T}_{ad}} \exp\left[\frac{1}{2}\tilde{T}_a\left(\frac{1}{\tilde{T}_{ad}} - \frac{1}{\tilde{T}_f}\right)\right] \tag{9}$$

This equation shows that when T_f approaches T_{ad} the mass flux at the reaction zone approaches the laminar flame value such that the burned velocity S_b is equal to S_b^o. Consequently, the unburned velocity S_u must exceed the laminar flame speed S_u^o. This effect is due entirely to flow divergence.

Computational and Experimental Studies - Methodology

Methane/air/inert mixtures were used in the studies. In the numerical simulation a version of the Sandia premixed flame code was used, with modifications to ensure strict mass conservation in the divergent flow field. The kinetic mechanism used was that developed by Egolfopoulos et al [8].

The experimental flat flame burner was made of a 5.1 cm diameter porous bronze disk with 20μm pore size and embedded cooling coils. Thermocouples were positioned inside the porous plug at known distances from the surface to measure the temperature gradient at the burner surface, from which the heat loss rate can be determined. During the experiments, the burner surface temperature was held at a constant value by varying the coolant flow rate. The inner and outer edges of the luminous zone of the flame were measured visually using a microscope. For detailed comparison, temperature profile through the flame was measured by using both thermocouples and Laser-Raman Spectroscopy. Experiments with the flat-flame burner were conducted under normal gravity conditions.

The cylindrical burner was made of a porous bronze tube with 5μm pore size, 1.25 cm diameter, and 3.76 cm active length. Due to the small burner size and the limited duration of the microgravity experiments, no cooling was used for the burner. A thermocouple was inserted inside the burner wall to record burner temperatures. Experiments were performed under microgravity conditions at the NASA-Lewis 2.2 second drop tower. Mass flow rates were measured using sonic flow nozzles and pressure transducers to record upstream pressures during the experiment. A video camera was used to record flame shapes and standoff distances.

Computational and Experimental Studies - Results

For the planar flame, Fig. 5 shows the optically-measured and computed temperature profiles across a ϕ=0.75 methane/air flame with a mass flow rate of 0.015 gm/cm^2-s. The comparison is fairly close, especially for the final temperature. This could imply that radiative heat loss, which is not included in the numerical calculations, is probably indeed unimportant for the weak flame investigated. The horizontal shift between the experimental and calculated profiles is about 0.25 mm. Since the flame location and thereby the temperature profile are fairly sensitive functions of the surface temperature, this shift could be due to a slight inaccuracy in the measured surface temperature.

Figure 6 compares the experimental and calculated flame standoff position and burner heat loss rate. For the numerical calculations the flame location was defined to be the position of maximum CH radical mole fraction, since this is the major species contributing to the flame luminosity. It is seen that the calculated flame standoff distance is smaller than the experimental values, with a correspondingly larger calculated heat loss rate. The overall level of agreement, however, can be considered to be satisfactory in view of the independent nature with which the calculation and experiments were conducted.

For the cylindrical flames, mixtures of $CH_4 + 2O_2 + 7.52\ N_2 + 5.665$ He, with an effective Lewis number of 2.2, were used for the experiments; helium was added to enhance flamefront stability [9]. The adiabatic flame temperature for the unburned mixture temperature of 300 K is 1885 K, and the calculated laminar burning rate is 17.1 cm/s, or 0.0135 gm/cm^2 s.

Figure 7 compares the calculated and measured flame standoff distance as a function of normalized mass flow M. Since the flames were not strictly cylindrical, the vertical bars of the experimental data show the range of the flame positions. The numerical results show that there is no heat loss to the burner at the flow rates shown in the figure. The comparison shows that for

high mass flow rates the calculated results are higher than the experimental values. The cause for this disagreement needs further study.

Summary

Microgravity cylindrical and spherical flames offer well-controlled flame configurations for fundamental studies of the structure and response of premixed and nonpremixed flames. Preliminary analytical, computational, and experimental studies demonstrate the viability of this approach.

Acknowledgments

This research was supported by the microgravity combustion program under NASA sponsorship. We appreciate the generous technical advice and assistance from K. Sacksteder and D. Dietrich at NASA-Lewis, and at Princeton University C. J. Sung and J. Liu.

References

1 Law, C. K. (1988). Dynamics of Stretched Flames. Twenty-Third Symposium (International) on Combustion, 1381.
2 Law, C. K. (1982). Recent Advances in Droplet Vaporization and Combustion. Prog. Energy. Combust. Sci. 8, 169.
3 Choi, M. Y., Dryer, F. L. and Haggard, J. (1991). Observations on a Slow Burning Regime for Hydrocarbon Droplets: n-heptane/Air Results. Twenty-Third Symposium (International) on Combustion, 1597.
4 Buckmaster, J. D. and Ludford, G. S. S. (1982). Theory of Laminar Flames. Cambridge Univ. Press, New York.
5 Ferguson, C. R. and Keck, J. C. (1979). Stand-Off Distances on a Flat Flame Burner. Combust. Flame 34, 85.
6 Spalding, D. B. and Yumlu, V. S. (1959). Experimental Demonstration of the Existence of Two Flame Speeds. Combust. Flame 3, 553.
7 Chao, B. H. and Law, C. K. (1988). Duality, Pulsating Instability, and Product Dissociation in Burner-Stabilized Flames. Combust. Sci. Tech. 62, 211.
8 Egolfopoulos, F. N., Zhu, D. L. and Law, C. K. (1990). Experimental and Numerical Determination of Laminar Flame Speeds: Mixtures of C_2-Hydrocarbons with Oxygen and Nitrogen. Twenty-Third Symposium (International) on Combustion, 471.
9 Matalon, M. and Matkowsky, B. J. (1983). Flames in Fluids: Their Interaction and Stability. Combust. Sci. Tech. 34, 295.

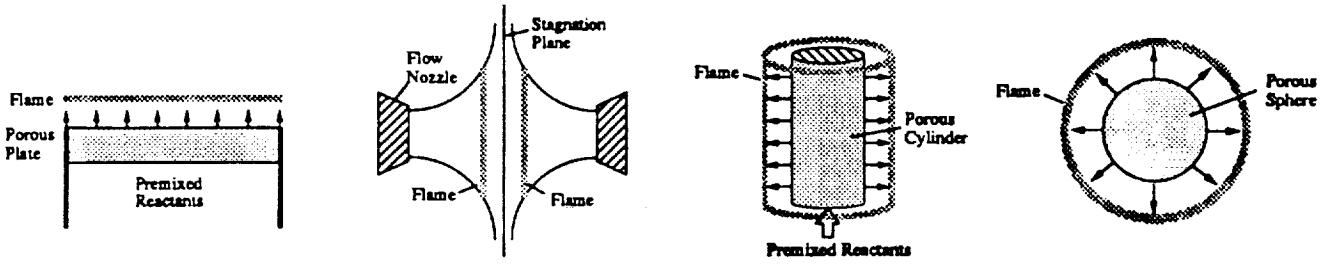

a) Flat Flame Burner b) Counterflow Burner c) Cylindrical Burner d) Spherical Burner

Figure 1

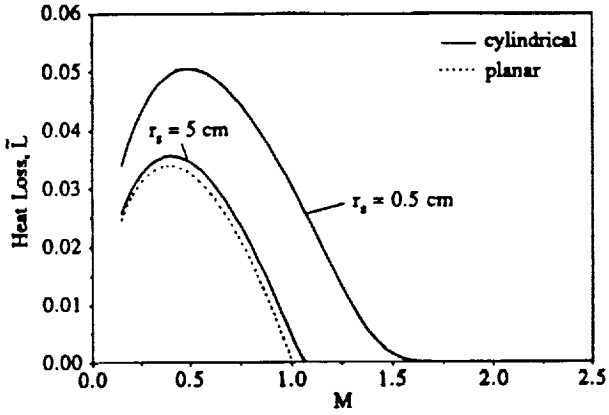

Figure 2

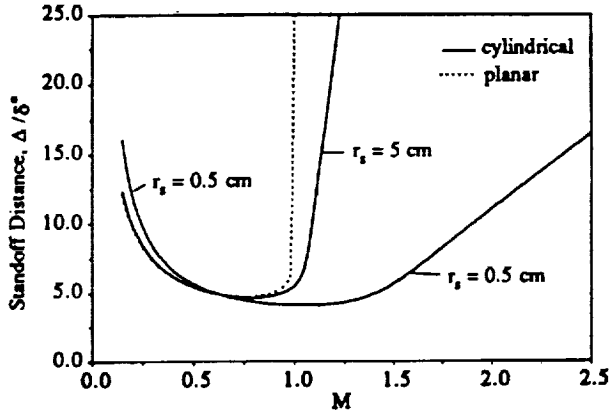

Figure 3

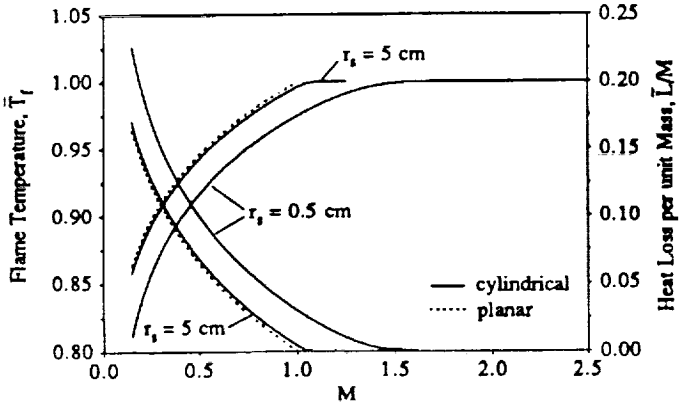

Figure 4

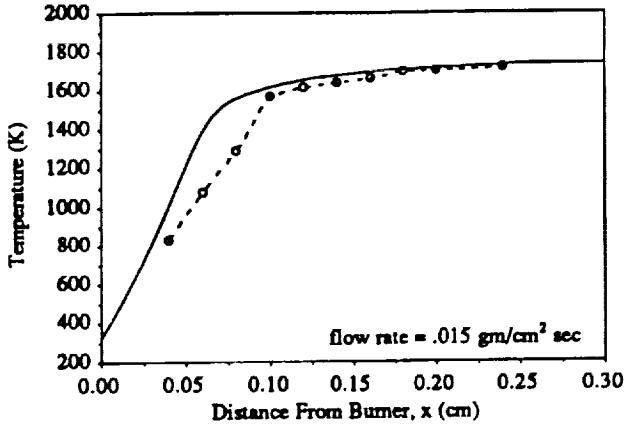

Figure 5

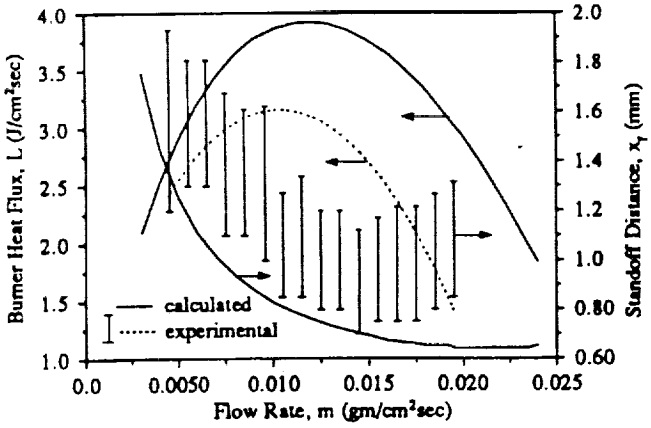

Figure 6

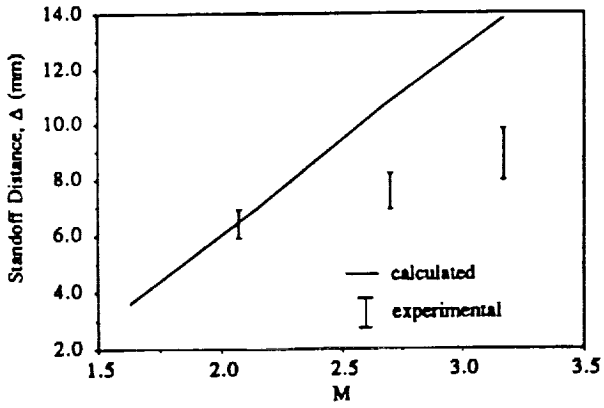

Figure 7

C-3